

# NONLINEAR PHENOMENA IN A MODEL SPACECRAFT POWER SYSTEM

Yan Hong Lim and David C. Hamill

Surrey Space Centre  
University of Surrey, Guildford, Surrey GU2 5XH, UK  
Tel. +44 (0) 1483 259278, Fax +44 (0) 1483 259503

Y.Lim@surrey.ac.uk D.Hamill@surrey.ac.uk

**Abstract** — We analyse a simple model of a spacecraft power system comprising a solar array, a filter and a model of a buck converter, by studying a set of third-order nonlinear differential equations. The analysis is based on nonlinear-dynamics concepts, which reveal bifurcation, hysteresis and chaos, and is supported by simulation results.

## I. INTRODUCTION

Dc power systems are almost universally used in small spacecraft such as satellites. This is because dc power is generated by solar arrays, batteries are used as energy reservoirs, and the payloads need dc supplies. The only exceptions are large spacecraft such as space stations, where high-frequency ac has been proposed for its ease of voltage transformation, important where large-scale distribution is required.

Space power systems incorporate dc-dc converters, and the switching devices and diodes within these make them inherently nonlinear. Power-system nonlinearities can lead to unpredictable behaviour. This is effectively revealed using nonlinear techniques, where linearisation methods fail [1–3].

A simple spacecraft power system has been studied by other workers, using state-plane analysis techniques [4]. That work was based on a second-order model comprising solar arrays (which have a nonlinear  $V$ - $I$  characteristic) with a second-order  $LC$  filter, coupled to a nonlinear load. The existence of multiple equilibrium points was discovered, and their stability investigated.

In the present paper, the model under study is a third-order nonlinear circuit comprising a solar array, a filter, a dc-dc converter and a dc load. This model also includes an undervoltage lockout circuit. Such circuits are commonly employed in space power systems to prevent the overdischarge of batteries during eclipse, or to ensure that converters operate in their proper mode so payloads receive a regulated voltage or no voltage at all. (Real spacecraft power systems are more complex, adding a battery, further regulators and power control switching.)

Third-order autonomous (i.e., free-running) nonlinear systems are particularly interesting, because they are the simplest systems capable of chaotic behaviour. Examples include the well known Lorenz and Rössler systems of

equations, and Chua’s circuit. As stated in [5],

‘Translated into circuit language, this means that ... [for chaos to occur in autonomous circuits] the presence of at least three reactive elements is required.’

We first derive from our model a set of three coupled first-order differential equations. We then introduce some of the nonlinear-dynamics packages we have used. In the remainder of the paper, we analyse the dynamics and carry out computer simulations with the aim of discovering any nonlinear behaviour, such as bifurcation and chaos.

## II. DERIVATION OF SYSTEM EQUATIONS

Fig. 1 shows a schematic of the system studied. It comprises a photovoltaic solar array, a third-order low-pass filter, a buck dc-dc converter and a resistive load. For the purpose of illustration, we assume that there is no battery and the spacecraft is powered in sunlight only. Further, we temporarily ignore the undervoltage lockout circuit and assume that the switch is always closed.

### A. Solar Array

The current  $i_1$  drawn from a solar array with impressed voltage  $v_1$  is usually described in the literature by an exponential characteristic derived from semiconductor physics. However, to model real solar arrays, we approximate the characteristic by the polynomial

$$i_1 = \alpha I_{sc} \left( 1 - \left( \frac{v_1}{V_{oc}} \right)^p \right) \quad 0 \leq v_1 \leq V_{oc}, \quad 0 \leq i_1 \leq I_{sc} \quad (1)$$

where  $p = 33$  gives a maximum error of 2%. Here,  $I_{sc}$  is the array’s short-circuit current,  $V_{oc}$  is its open-circuit voltage, and  $\alpha$  is a factor denoting the relative solar illumination ( $0 \leq \alpha \leq 1$ ). Note that the current  $i_1$  and voltage  $v_1$  cannot

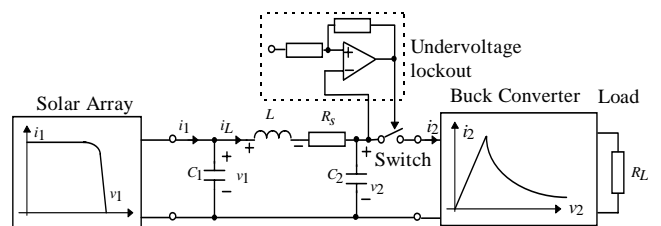


Fig 1: Simplified model of a spacecraft power system.

exceed  $I_{sc}$  and  $V_{oc}$  respectively. This equation is valid for the voltage and current ranges shown, which are those found in normal operation.

### B. Dc-Dc Converter and Load

The buck dc-dc converter is assumed to be lossless and to operate in continuous conduction mode. The converter's dc load is represented by a constant resistance  $R_L$ . During the satellite's orbit in space, the solar array voltage varies, causing the voltage to the input of the converter to vary too. Because of this, the buck dc-dc converter has two modes of operation, one desirable, the other undesirable. When there is sufficient voltage from the solar array, the output is regulated and constant — this is desirable and the input characteristic is a constant-power hyperbola. However, if the input voltage is insufficient, the output becomes unregulated and a constant-resistance characteristic results, which is undesirable. Thus the overall converter's input characteristic is described by

$$i_2(v_2) = \begin{cases} \frac{V_{ref}^2}{R_L v_2} & \text{if } v_2 \geq V_{ref} \quad (\text{desirable}) \\ \frac{v_2}{R_L} & \text{if } v_2 < V_{ref} \quad (\text{undesirable}) \end{cases} \quad (2)$$

where  $v_2$  and  $i_2$  are the input voltage and current to the converter respectively and  $V_{ref}$  is the desired voltage at the output.

### C. Third-Order Filter

The filter used in the system comprises two capacitors  $C_1$  and  $C_2$  and an inductor  $L$ . Capacitor  $C_1$  includes the parasitic capacitance of the solar array,  $L$  includes wiring inductance, and  $C_2$  is the input capacitor needed for any practical buck converter. We represent parasitic losses by the resistance  $R_s$ . (The dynamics of dissipative systems differ from those of lossless systems, also known as conservative or Hamiltonian systems.)

### D. System Equations

Combining these models with the state equations for  $C_1$ ,  $L$  and  $C_2$ , we obtain an autonomous, coupled set of three nonlinear differential equations which govern the dynamics of the model spacecraft power system:

$$\left. \begin{aligned} \frac{dv_1}{dt} &= \frac{i_1(v_1) - i_L}{C_1} &= f_1(v_1, i_L, v_2) \\ \frac{di_L}{dt} &= \frac{v_1 - i_L R_s - v_2}{L} &= f_2(v_1, i_L, v_2) \\ \frac{dv_2}{dt} &= \frac{i_L - i_2(v_2)}{C_2} &= f_3(v_1, i_L, v_2) \end{aligned} \right\} \quad (3)$$

## III. COMPUTER SIMULATION PACKAGES

In our work to date, we have employed the following simulation approaches. There are many other dynamical-

system simulation packages apart from those listed below, including *DStool* [6], *INSITE* [7], and *MATLAB* with *Simulink* [8].

### A. XPP-Aut

*XPP-Aut* (X-Windows Phase Plane plus Auto) [9] is a user-friendly dynamical-systems tool that runs on UNIX workstations, and is free of charge. XPP can be used to solve differential and difference equations and to produce two and three-dimensional phase-space plots. It also has an interface that allows data produced by its differential-equation solver to be fed to the bifurcation-analysis package AUTO [10]. In its original form, AUTO is a stand-alone program which is given an autonomous set of differential or difference equations to solve, and a parameter to vary. Using numerical continuation techniques, it locates branches of equilibrium points and periodic solutions, and evaluates their stability. This allows us to obtain a general view of the global behaviour of a nonlinear system.

XPP-Aut can compute bifurcation diagrams and Poincaré sections, amongst other things. It is a powerful and user-friendly simulation package. XPP-Aut is the main tool in our simulations. However, systems with discontinuities (and this includes all power-electronic systems) may present numerical problems to AUTO.

### B. VisSim

*VisSim* [11] is a typical block-diagram oriented dynamical-systems package. It offers a straightforward method for modelling and simulating dynamical systems. Linear, nonlinear, continuous-time, discrete-time, time-varying and hybrid system designs are also supported, as well as neural networks and fuzzy logic. It is basically a differential-equation solver. Although it does not allow global system behaviour to be identified, it does allow the user to observe the effects of changing parameter values in real time. This is a commercial package.

### C. PSpice

*PSpice* [12] is a well known commercial circuit-simulation package, derived from the public-domain *SPICE* (Simulation Program with Integrated Circuit Emphasis) [13]. It runs on IBM-PCs. Evaluation versions are readily available free of charge. In early versions, which run under MS-DOS, the user creates a netlist file with a text editor. Evaluation version 5.0 has been used to verify chaotic behaviour in a variety of nonlinear circuits [14]. In later versions, which run under MS-Windows, the input file is generated automatically via a drag-and-drop graphical user interface.

Although PSpice is a powerful package, it is essentially a circuit simulator. To model a system represented by equations or functional blocks, an equivalent electrical network must be produced. This frequently requires considerable ingenuity. Moreover, few nonlinear functions are offered.

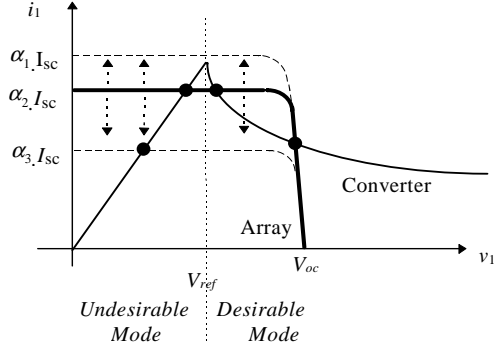


Fig. 2: Converter and solar array  $V$ - $I$  characteristics with varying illumination factor  $\alpha$ .

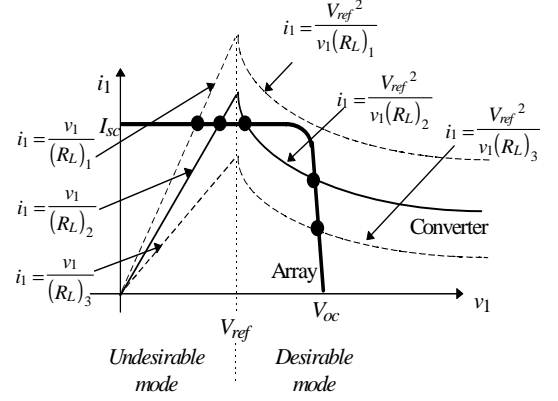


Fig. 3: Converter and solar array  $V$ - $I$  characteristics with varying load resistance  $R_L$ .

PSpice is best suited to circuit-level studies.

#### D. Hand-Coded Programs

Coding in a high-level language such as C, FORTRAN or Pascal offers the user high-speed simulation and improved flexibility. Standard packages can have serious shortcomings: for example, the functions provided may be inadequate to describe a system, or the facilities for manipulating data may be limited. For example, to obtain the results of Section VI below, we wrote our own C code for the following reasons: 1) to include a hysteresis function easily; 2) to generate bifurcation diagrams and Poincaré sections conveniently; and 3) to speed up simulation so the diagrams could be produced in a reasonable time. However, it must be pointed out that hand-coding inevitably introduces bugs, which may give misleading results. Findings should always be validated by corroborative evidence from other sources.

### IV. EQUILIBRIUM POINTS

To find the system's equilibrium points, we follow the usual method of setting the derivatives of all the state variables simultaneously to zero, i.e. setting  $f_1 = f_2 = f_3 = 0$  in (3). This reduces the system to its rest state. We obtain

$$i_1(v_1) = i_L; \quad v_1 = i_L R_s + v_2; \quad i_L = i_2(v_2) \quad (4)$$

In the undesirable mode, with (2) and (4),  $i_L^* = i_2^* = v_2^*/R_L$ . (We denote the steady-state values by an asterisk.) Thus  $v_1^* = i_L^*(R_L + R_s)$  and the equilibrium point  $i_L^*$  can be obtained by solving

$$i_L^* = I_{sc} \alpha \left( 1 - \left( \frac{i_L^*(R_s + R_L)}{V_{oc}} \right)^p \right) \quad (5)$$

Back-substituting, we obtain the other equilibrium state variables from  $v_2^* = i_L^* R_L$  and  $v_1^* = v_2^* + i_L^* R_s$ .

In the desirable mode,  $i_2^* = i_L^* = V_{ref}^2 / (v_2^* R_L)$ . Therefore

$$i_L^* = I_{sc} \alpha \left( 1 - \left( \frac{\frac{V_{ref}^2}{R_L i_L^*} + i_L^* R_s}{V_{oc}} \right)^p \right) \quad (6)$$

with  $v_2^* = V_{ref}^2 / i_L^* R_L$  and  $v_1^* = v_2^* + i_L^* R_s$ .

Equilibrium points occur where the two dc  $V$ - $I$  characteristics intersect, indicated in Fig. 2 by dots. The number of equilibrium points depends on various parameters, such as the illumination (Fig. 2) and the load (Fig. 3).

The mathematics may produce spurious equilibria (e.g.  $A_1$  and  $A_2$  in Fig. 4) outside the valid range of each operating mode, so every equilibrium point must be checked for validity. There may be one, two or three valid equilibrium points, depending on the parameter values.

### V. STABILITY OF EQUILIBRIA

#### A. Eigenvalues of the Jacobian

The stability of each equilibrium point can be investigated by examining the eigenvalues  $\{\lambda_1, \lambda_2, \lambda_3\}$  of the Jacobian matrix  $\mathbf{J}$  of the system at equilibrium, given by

$$\mathbf{J} = \begin{bmatrix} df_1/dv_1 & df_1/di_L & df_1/dv_2 \\ df_2/dv_1 & df_2/di_L & df_2/dv_2 \\ df_3/dv_1 & df_3/di_L & df_3/dv_2 \end{bmatrix}_{v_1^*, i_L^*, v_2^*} \quad (7)$$

Substituting (3) into (7),

$$\mathbf{J} = \begin{bmatrix} \frac{-I_{sc} \alpha p v_1^{p-1}}{V_{oc}^p C_1} & -\frac{1}{C_1} & 0 \\ \frac{1}{L} & -\frac{R_s}{L} & -\frac{1}{L} \\ 0 & \frac{1}{C_2} & \frac{V_{ref}^2}{R_L C_2 v_2^2} \end{bmatrix}_{v_1^*, i_L^*, v_2^*} \quad (8)$$

when the switch is closed and

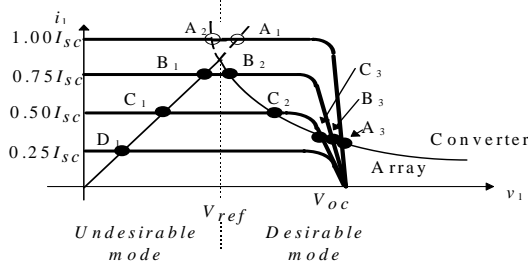


Fig 4:  $V$ - $I$  characteristics, showing valid equilibrium states (filled dots) and invalid states  $A_1$  and  $A_2$  (open dots) with varying illumination factor  $\alpha$ .

$$\mathbf{J} = \begin{bmatrix} -\frac{I_{sc}\alpha p v_1^{p-1}}{V_{oc}^p C_1} & -\frac{1}{C_1} & 0 \\ \frac{1}{L} & -\frac{R_s}{L} & -\frac{1}{L} \\ 0 & \frac{1}{C_2} & 0 \end{bmatrix} \quad (9)$$

when the switch is open.

We investigate quantitatively an example using the following parameter values:  $I_{sc} = 4\text{A}$ ,  $V_{oc} = 46.2\text{V}$ ,  $V_{ref} = 14\text{V}$ ,  $R_s = 3.92\Omega$ ,  $L = 700\mu\text{H}$ ,  $C_1 = 350\mu\text{F}$  and  $C_2 = 50\mu\text{F}$ . Four cases are considered, from  $\alpha = 0.25$  to  $1.00$  (full illumination). Table I shows numerical results, obtained using the Maple V symbolic algebra package.

For each value of  $\alpha$ , equilibrium points obtained from (5) and (6) are shown. Although there are three computed equilibrium points for  $\alpha = 1$  ( $A_1$ ,  $A_2$  and  $A_3$ ), only one is valid:  $A_3$ . The invalid ones are shaded. (At  $A_2$ ,  $v_2^* = 12.500\text{V}$  violates the condition  $v_2^* \geq V_{ref}$  and at  $A_1$ ,  $v_2^* = 15.680\text{V}$  violates  $v_2^* < V_{ref}$ .) For  $\alpha = 0.75$  and  $0.50$ , all three equilibria are valid. For  $\alpha = 0.25$ , there are no equilibrium points in the desirable mode because the dc-characteristics do not intersect. This is clarified in Fig. 4, which indicates the valid and invalid equilibria.

To examine the stability, the eigenvalues for the eight valid equilibria were found numerically with Maple, and

Table I: Equilibrium points.

Undesirable mode ( $v_2 < V_{ref}$ )						
$\alpha$	Label	$i_1^*$	$v_1^*$	$i_L^*$	$v_2^*$	$i_2^*$
0.25	D <sub>1</sub>	1.00	4.12	1.00	3.92	1.00
0.50	C <sub>1</sub>	2.00	8.24	2.00	7.84	2.00
0.75	B <sub>1</sub>	3.00	12.36	3.00	11.76	3.00
1.00	A <sub>1</sub>	4.00	16.48	4.00	15.68	4.00
Desirable mode ( $v_2 \geq V_{ref}$ )						
$\alpha$	Label	$i_1^*$	$v_1^*$	$i_L^*$	$v_2^*$	$i_2^*$
0.25	—	—	—	—	—	—
0.50	C <sub>2</sub>	2.00	25.40	2.00	25.00	2.00
	C <sub>3</sub>	1.114	45.10	1.114	44.88	1.114
0.75	B <sub>2</sub>	3.00	17.72	3.00	16.67	3.00
	B <sub>3</sub>	1.102	45.67	1.102	45.45	1.102
1.00	A <sub>2</sub>	4.00	13.30	4.00	12.50	4.00
	A <sub>3</sub>	1.098	45.75	1.098	45.53	1.098

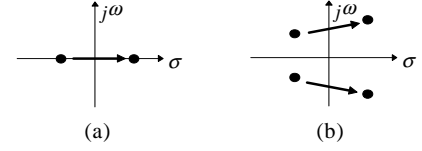


Fig. 5: (a) Stationary bifurcation; (b) Hopf bifurcation.

are listed in Table II.

For  $\alpha = 0.75$  and  $0.50$ , there are three equilibria in each case, two of which are stable ( $B_1$ ,  $B_3$  and  $C_1$ ,  $C_3$  respectively) and one unstable ( $B_2$  and  $C_2$  respectively). The unstable ones have an eigenvalue in the right half-plane. For  $\alpha = 0.25$  and  $1.00$ , the single equilibrium is stable, the eigenvalues having negative real parts.

### B. Stationary Bifurcation

As the illumination intensity is decreased, the single equilibrium at  $A_3$  suddenly changes into three equilibria  $B_1$ ,  $B_2$  and  $B_3$  in Fig. 4. This happens as  $\lambda_3$  moves along the real axis into the right half-plane, as shown in Fig. 5(a). This is known as a *stationary bifurcation* [15]. (A *bifurcation* is a qualitative change in system behaviour as a parameter is varied.)

### C. Hopf Bifurcation

Hopf bifurcation is also possible in this system. A Hopf bifurcation differs from a stationary bifurcation in that a pair of complex conjugates crosses the imaginary axis into the right half-plane (Fig. 5(b)). This is evident when we observe the complex eigenvalues  $\{\lambda_1, \lambda_2\}$  of  $B_2$  (and likewise  $C_2$ ), whose real part becomes positive. At the point where the real part of the complex conjugates changes sign, a Hopf bifurcation occurs: there is a simple pair of purely imaginary eigenvalues. Hopf bifurcations give rise to periodic solutions. In nonlinear dynamical systems, these periodic solutions may induce phenomena such as limit cycles, quasi-periodicity and chaos.

Table II: Eigenvalues of the Jacobian at equilibrium points.

$\alpha$	Label	Eigenvalues			Stability
		$\lambda_1$	$\lambda_2$	$\lambda_3$	
0.25	D <sub>1</sub>	-2357.3	-2357.3	-673.1	stable
		-j5037.9	+j5037.9		
0.50	C <sub>1</sub>	-2357.3	-2357.3	-673.1	stable
		-j5037.9	+j5037.9		
	C <sub>2</sub>	+555.0	+555.0	+204.2	unstable
		-j5626.8	+j5626.8		
	C <sub>3</sub>	-31.8	-31.8	-1613.2	stable
		-j5657.9	+j5657.9		
0.75	B <sub>1</sub>	-2357.3	-2357.3	-673.1	stable
		-j5037.9	+j5037.9		
	B <sub>2</sub>	+1413.7	+1413.7	+485.5	unstable
		-j5315.4	+j5315.4		
	B <sub>3</sub>	-101.5	-101.5	-3820.8	stable
		-j5557.6	+j5557.6		
1.00	A <sub>3</sub>	-106.8	-106.8	-5232.7	stable
		-j5502.3	+j5502.3		

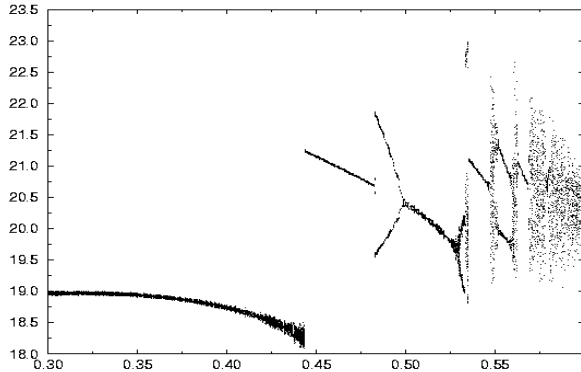


Fig. 6: Bifurcation diagram of  $v_2$  against  $\alpha$ , showing hysteresis and subcritical Hopf bifurcations. Filled dots represent stable periodic orbits; open dots represent unstable periodic orbits.

Fig. 8: Bifurcation diagram of  $v_2$  against  $\alpha$  with initial conditions  $v_1 = 20V$ ,  $i_L = 1A$ ,  $v_2 = 20V$ . Turning point at  $\alpha = 0.8998$ .

To investigate this further, the system equations of (3) incorporating (2) were investigated numerically using XPP-Aut. AUTO tracks the solutions and their associated stability as we vary a system parameter (the *bifurcation parameter*).

To emulate a satellite's changing illumination level,  $\alpha$  was selected as the bifurcation parameter. Fig. 6 (a *bifurcation diagram*) shows how the buck-converter equilibrium voltages  $\{v_2\}$  vary as  $\alpha$  changes.

#### D. Hysteresis

Two interesting illumination levels are at  $\alpha = 0.3113$  and  $\alpha = 0.8998$ . These values delimit a range in which two values of array voltage are stable and one is unstable. At the extremes of this range, a pair of equilibria merge and vanish. Within the range, either of the two stable equilibria could be chosen, depending on the initial conditions. A large disturbance might flip the system to its other stable equilibrium. This phenomenon is well known as *hysteresis*.

If  $R_L$  is taken as the bifurcation parameter instead of  $\alpha$ , which is set to 1.00, the range  $1.236\Omega < R_L < 3.488\Omega$  is now associated with hysteresis.

In normal operation, as either  $\alpha$  or  $R_L$  (or both) vary, the system will move to the lower stable branch if there is insufficient illumination for the load power demanded. This is known as *voltage collapse* and is a notorious hazard of spacecraft power system operation. To escape from it,  $R_L$  has to be increased (beyond  $3.488\Omega$  at full illumination) by turning off payloads, an operation known as *load shedding*.

#### E. Self-Oscillation and Coexisting Attractors

There are two further interesting values of illumination:  $\alpha = 0.4534$  and  $\alpha = 0.8997$ , which are known as Hopf points. Starting at these points, AUTO traces the branches of the

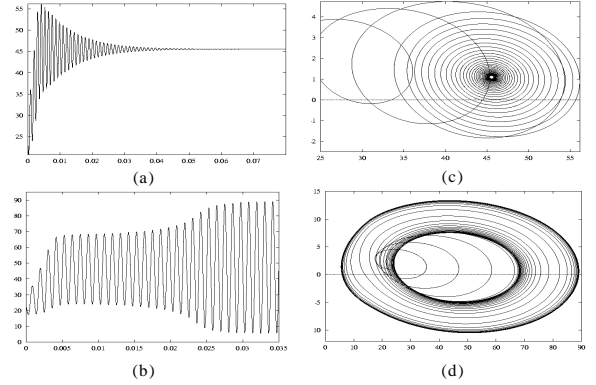


Figure 7: At  $\alpha = 1$ , (a) and (b) are waveforms of  $v_2$ , (c) and (d) are state-plane trajectories of  $v_2$  against  $i_L$ . With different initial conditions; (a) and (c) show a stable equilibrium, (b) and (d) a limit cycle.

periodic solutions, which can be either stable (limit cycles) or unstable (ringing).

In Fig. 6, filled dots denote stable periodic solutions and unfilled dots, unstable ones. *Subcritical Hopf bifurcations* are revealed as periodic-solution branches emanate from the stable-equilibrium branches. Unstable at first, they turn and become stable (limit cycles). In the range  $0.4534 < \alpha < 0.8997$ , three attractors coexist: two stable equilibria and a stable limit cycle. (An *attractor* is a stable limit set. A *limit set* is the set of points visited by the state vector in the limit as  $t \rightarrow \infty$ .) There are also two unstable periodic solutions and an unstable equilibrium, making for very complex transient dynamics.

The range  $\alpha > 0.35$  is of particular engineering concern, because besides the desired stable equilibria, stable limit cycles exist, perhaps unsuspected. Suppose the system is operating as intended, on the upper stable equilibrium branch at  $\alpha = 1$ , say. With a large perturbation, the system might cross into the basin of attraction of the limit cycle (its 'catchment region'), bursting into sustained large-amplitude oscillation (see Fig. 7). Coexisting attractors of this type are a serious threat to reliable operation, and might cause malfunctions, or even failure.

## VI. COEXISTING LIMIT CYCLES AND CHAOS

Next, we introduce the undervoltage lockout circuit into the system. The reason is now apparent: we want to prevent the system from operating in the undesirable mode, to avoid the above effects.

The lockout circuit has its own hysteresis, included to prevent switch chattering. When  $v_2$  falls below a preset threshold, the switch opens and disconnects the converter's input. The switch remains open while the solar array charges the capacitors. When the voltage across  $C_2$  rises above a higher preset threshold, the switch closes and reconnects the converter.

Instead of (2), we now have

$$i_2 = \begin{cases} 0 & \text{if } v_2 \leq V_{lo} \text{ (switch open)} \\ V_{ref}^2 / R_L v_2 & \text{if } v_2 \geq V_{up} \text{ (switch closed)} \end{cases} \quad (10)$$

where  $V_{lo} = 19\text{V}$  and  $V_{up} = 21\text{V}$  are the preset lower and upper thresholds respectively. If  $V_{lo} < v_2 < V_{up}$ , the switch state is unchanged, and  $i_2$  takes the corresponding value.

The capacitance values used are now  $C_1 = 50\mu\text{F}$  and  $C_2 = 350\mu\text{F}$ , the other parameter values being unchanged.

### A. Bifurcation Diagrams

To investigate the system dynamics qualitatively, we again look to the bifurcation diagrams. Figs. 8 and 9 show

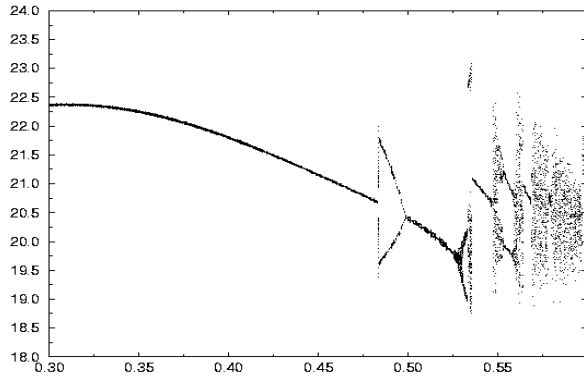


Fig. 9: Bifurcation diagram of  $\{v_1\}$  against  $\alpha$  with initial conditions:  $v_1 = 20.9\text{V}$ ,  $i_L = 1\text{A}$ ,  $v_2 = 20.9\text{V}$ .

bifurcation diagrams of  $\{v_1^*\}$  against  $\alpha$ . For each  $\alpha$  sampled in the range  $0.3 \leq \alpha < 0.6$ ,  $\{v_1^*\}$  is the collection of the values of  $v_1$  repeatedly captured each time the trajectory touches the planar surface at  $v_2 = 21\text{V}$  (the upper threshold). This value was chosen for convenience; sampling other state variables would give qualitatively similar results.

Instead of using a simulation package, we implemented this in the C programming language, to increase simulation speed and improve flexibility. The simulations used a fixed  $1\mu\text{s}$ -timestep fifth-order Runge-Kutta integration routine. The bifurcation diagrams of Fig. 8 and 9 were generated using two different initial conditions, and this revealed the coexistence of two limit cycles (see Fig. 10(a)) for  $\alpha = 0.3$  to  $0.443$ , each having its own basin of attraction. At  $\alpha = 0.443$ , the attractor of Fig. 9 dominates. For  $\alpha > 0.443$ , the two diagrams are identical. At  $\alpha = 0.483$ , a period-2 limit cycle emerges, associated with a chaotic transient. It converges back to period-1 at  $\alpha = 0.5$  but splits again into period-2 at  $\alpha = 0.528$ . At  $\alpha = 0.535$ , a tiny band of chaos is observed.

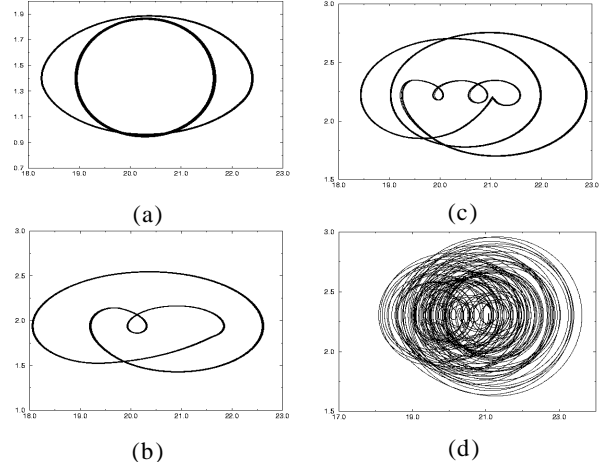


Fig. 10: State-plane trajectories of  $v_1$  against  $i_L$  showing (a) coexisting limit cycles at  $\alpha = 0.35$ , (b)  $\alpha = 0.485$ , (c)  $\alpha = 0.555$ , (d) chaotic attractor at  $\alpha = 0.576$ .

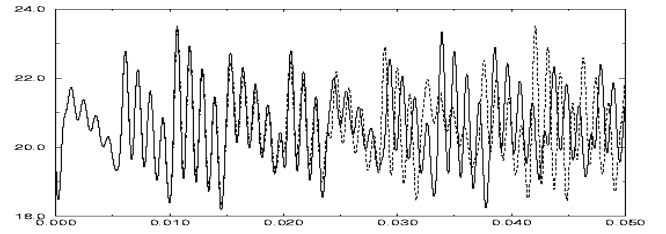


Fig. 11: Chaotic time waveform of  $v_1$  at  $\alpha = 0.576$ , showing sensitive dependence on initial conditions.

*Chaos* still lacks a universally accepted definition. Loosely speaking, it is a noise-like oscillation (having a broadband spectrum) that occurs in deterministic systems. The chaotic trajectory is very sensitive to perturbations, but remains within a bounded region of state space. Chaos is associated with infinitely complex fractal structures known as *strange attractors*.

As  $\alpha$  is increased, we witness further bands of chaos interspersed with period-doubling; from  $0.576 \leq \alpha \leq 0.6$ , chaos reigns. With  $\alpha \geq 0.6$ , the illumination is adequate for the switch to close continuously; thus operation reverts to a stable equilibrium in the desirable mode.

### B. Evidence for Chaos

Fig. 10 shows the state-plane trajectories of  $v_1$  plotted against  $i_L$  for various illuminations  $\alpha$ . Fig. 11 illustrates sensitive dependence on initial conditions: with just  $0.02\text{V}$  difference, the waveforms, at first nearly identical, soon diverge and become uncorrelated.

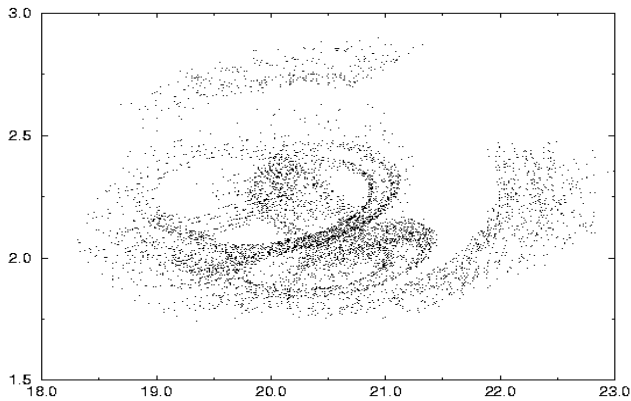


Fig. 12: Poincaré section at  $v_2 = 20\text{V}$  with  $v_1$  plotted against  $i_L$ , for  $\alpha = 0.576$ .

The Poincaré section of Fig. 12 was constructed by plotting  $\{(v_1, i_L)\}$  sampled at  $v_2 = 20\text{V}$ . The fractal nature of this attractor is further evidence of chaos.

## VII. VERIFICATION WITH VisSim

The system is next simulated with VisSim [9], using the same parameters and operating conditions. Fig. 13 shows the system block-diagram model, and simulation results for chaotic operation at  $\alpha = 0.576$ . The state-plane trajectories are in agreement with those previously obtained.

## VIII. CONCLUSION

In summary, a simple spacecraft power system has been studied analytically and numerically, using computer algebra and nonlinear dynamics software. The presence of stationary and Hopf bifurcation were confirmed; and simulation results reveal typical nonlinear behaviour: hysteresis, limit cycles, coexisting attractors, period-multiplication and chaos.

## ACKNOWLEDGEMENT

The authors acknowledge the assistance of Y. Hashida.

## REFERENCES

[1] Hamill, D.C.: Power electronics: a field rich in nonlinear dynamics. *Workshop on Nonlinear Dynamics of Electronic Systems*, Dublin, July 1995, pp. 164–179.

[2] Chiang, H.D., Liu, C.W., Varaiya, P.P., Wu, F.F., Lauby, M.G.: Chaos in a simple power system. *IEEE Trans. on Power Systems*, vol. 8, no. 4, , Nov. 1993, pp. 1407–1417.

[3] Wang, H.O., Abed, E.H., Hamdan, A.M.A.: Bifurcations, chaos, and crises in voltage collapse of a model power system. *IEEE Trans. on Circuits and Systems, Part I*, vol. 41,

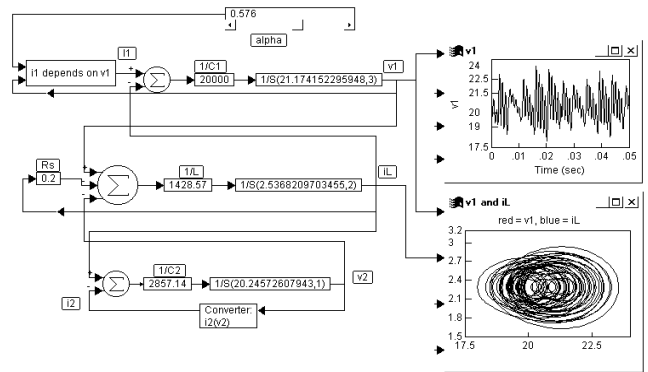


Fig 13: System simulation with VisSim.

no. 4, Mar. 1994, pp. 294–302.

- [4] Cho, B.H.; Lee, J. R.; Lee, F.C.: Large-signal stability analysis of spacecraft power processing systems. *Power Electronics Specialists Conf.*, 1987, pp. 289–294.
- [5] Hasler, M.J.: Electrical circuits with chaotic behaviour. *Proc. IEEE*, vol. 75, no. 8, Aug. 1987, pp. 1009–1021.
- [6] Guckenheimer, J.; Myers, M.R.; Wicklin, F.J.; Worfolk, P.A.: *DStool: Dynamical System Toolkit with Interactive Graphic Interface*. Center for Applied Mathematics, Cornell Univ., 1991. (<ftp://macomb.tn.cornell.edu/pub/dstool/>).
- [7] Parker, T.S.; Chua, L.O.: *Practical Numerical Algorithms for Chaotic Systems*. New York, Springer-Verlag, 1988. (INSITE: Interactive Nonlinear Systems Investigative Toolkit for Everyone).
- [8] The MathWorks Inc. (<http://www.mathworks.com>).
- [9] Ermentrout, B.: *XPPAUT 3.8*. Univ. of Pittsburg. (<http://www.pitt.edu/~phase/>).
- [10] Doedel, E.: *AUTO*. Concordia Univ. (<ftp://ftp.cs.concordia.ca/pub/doedel/auto/>).
- [11] Visual Solutions Inc. (<http://www.vissim.com>).
- [12] Tuinenga, P.W.: *Spice, A Guide to Circuit Simulation and Analysis Using PSpice*. Prentice-Hall, 1988.
- [13] Nagel, L.W.: *SPICE2: a computer program to simulate semiconductor circuits*. Electronics Res. Lab. Memo. ERL-M520, College of Eng., Univ. of California, Berkeley, CA, 1975.
- [14] Hamill, D.C.: Learning about chaotic circuits with SPICE. *IEEE Trans. on Education*, vol. 36, no. 1, Feb. 1993, pp. 28–35.
- [15] Seydel, R.: *From Equilibrium to Chaos: Practical Bifurcation and Stability Analysis*. Elsevier Science Publishing, 1988.